Localized recruitment and activation of RhoA underlies dendritic spine morphology in a glutamate receptor–dependent manner

Vanessa Schubert,[1] Jorge Santos Da Silva,[1] and Carlos G. Dotti[1,2,3]

[1]Cavalieri Ottolenghi Scientific Institute, Universita Degli Studi di Torino, Azienda Ospedaliera San Luigi Gonzaga, Regione Gonzole 10, 10043 Orbassano (Torino), Italy
[2]Department of Human Genetics, Catholic University of Leuven, 3000 Leuven, Belgium
[3]Flanders Interuniversity Institute of Biotechnology, 3000 Leuven, Belgium

Actin is the major cytoskeletal source of dendritic spines, which are highly specialized protuberances on the neuronal surface where excitatory synaptic transmission occurs (Harris, K.M., and S.B. Kater. 1994. *Annu. Rev. Neurosci.* 17:341–371; Yuste, R., and D.W. Tank. 1996. *Neuron.* 16:701–716). Stimulation of excitatory synapses induces changes in spine shape via localized rearrangements of the actin cytoskeleton (Matus, A. 2000. *Science.* 290:754–758; Nagerl, U.V., N. Eberhorn, S.B. Cambridge, and T. Bonhoeffer. 2004. *Neuron.* 44:759–767). However, what remains elusive are the precise molecular mechanisms by which different neurotransmitter receptors forward information to the underlying actin cytoskeleton. We show that in cultured hippocampal neurons as well as in whole brain synaptosomal fractions, RhoA associates with glutamate receptors (GluRs) at the spine plasma membrane. Activation of ionotropic GluRs leads to the detachment of RhoA from these receptors and its recruitment to metabotropic GluRs. Concomitantly, this triggers a local reduction of RhoA activity, which, in turn, inactivates downstream kinase RhoA-specific kinase, resulting in restricted actin instability and dendritic spine collapse. These data provide a direct mechanistic link between neurotransmitter receptor activity and the changes in spine shape that are thought to play a crucial role in synaptic strength.

Introduction

Synaptic transmission efficacy largely depends on the morphology of dendritic spines, which are highly specialized protrusions on the neuronal surface that receive most of the central excitatory input (Harris and Kater, 1994; Yuste and Tank, 1996). Dendritic spines are highly motile structures capable of undergoing rapid morphological plasticity in response to external signaling events (Bonhoeffer and Yuste, 2002; Nimchinsky et al., 2002). Such architectural changes are achieved via dynamic modifications of the local actin cytoskeleton, the major cytoskeletal element present in dendritic spines (Fifkova and Delay, 1982; Matus et al., 1982; Matus, 2000).

Correspondence to Carlos G. Dotti: carlos.dotti@med.kuleuven.be

J.S. Da Silva's present address is Cold Spring Harbor Laboratory, Cold Spring Harbor, NY 11724.

Abbreviations used in this paper: Dia1, Diaphanous 1; F-actin, filamentous actin; GDP, guanosine diphosphate; GluR, glutamate receptor; iGluR, ionotropic GluR; mGluR, metabotropic GluR; NMDA, *N*-methyl-D-asparate; NMDAR, NMDA receptor; PIIa, profilinIIa; PSD, postsynaptic density; ROCK, RhoA-specific kinase; ST, synaptotagmin.

The online version of this article contains supplemental material.

Much information has been gathered describing the many actin-regulatory mechanisms that cells use to control diverse morphogenic events (Luo, 2002). A group of proteins that have acquired a most noticeable position are the Rho GTPases, of which RhoA, Rac1, and cdc42 are the best-characterized members (Hall, 1998; Settleman, 1999). Rho GTPases act as molecular switches, existing in an active GTP-bound and an inactive guanosine diphosphate (GDP)–bound state (Van Aelst and D'Souza-Schorey, 1997; Hall, 1998). Depending on this, these proteins trigger modifications in the actin polymerization state via specific downstream effectors. As they are ubiquitously distributed, the activity of Rho GTPases must be precisely monitored in space and time, allowing for the many different architectural actin-dependent modifications occurring at different cellular domains (Govek et al., 2005). Thus, for example, the protrusive or quiescent status of axonal growth cones is determined by the dynamic state of the underlying actin cytoskeleton, which, in turn, is locally regulated by specific membrane-signaling events in a Rho GTPase–dependent manner (Luo, 2000). In principle, a similar spatially and temporally

The Journal of Cell Biology, Vol. 172, No. 3, January 30, 2006 453–467
http://www.jcb.org/cgi/doi/10.1083/jcb.200506136

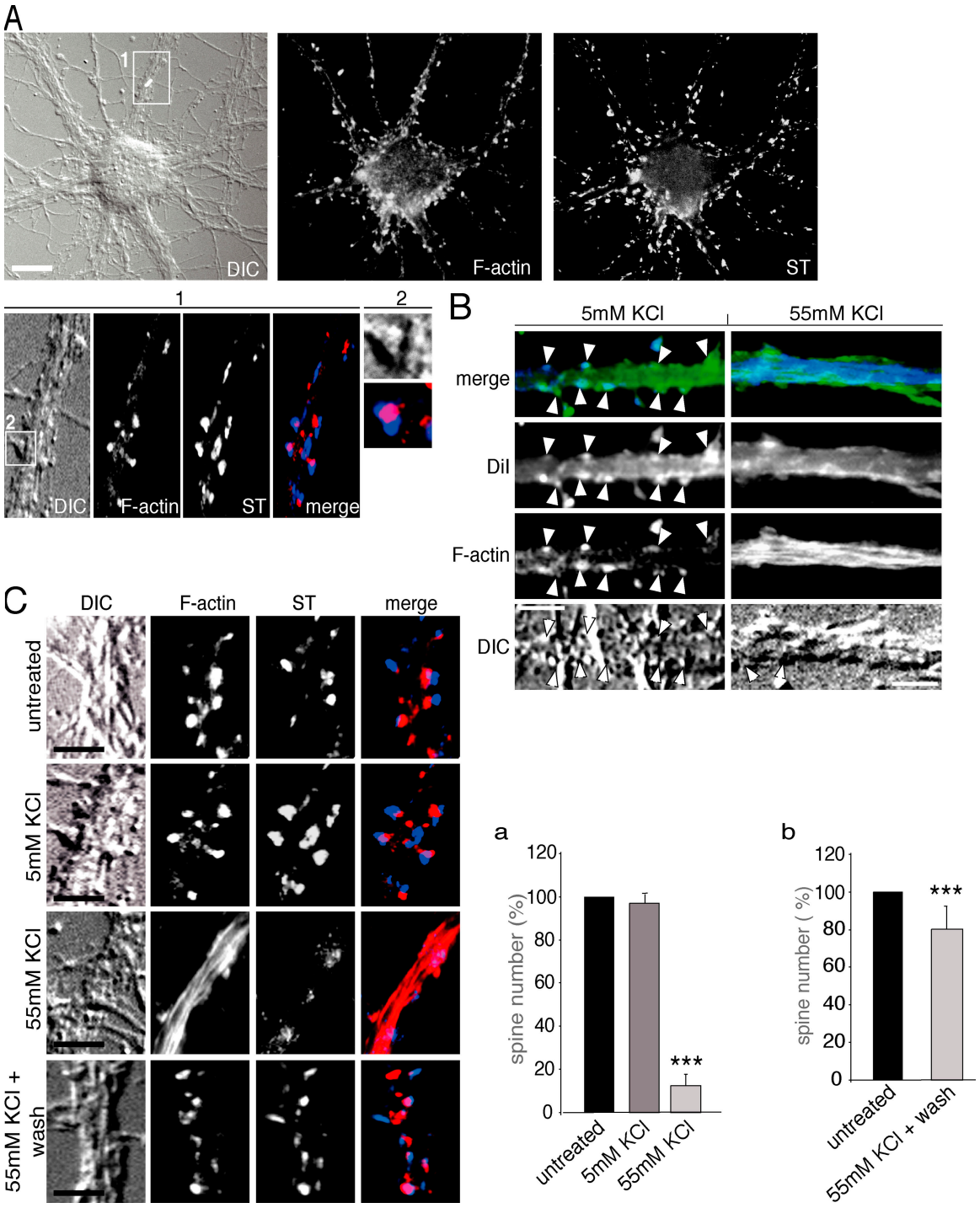

Figure 1. **High concentrations of KCl lead to local depolymerization of F-actin and dendritic spine retraction.** (A) Dendritic spines were visualized with phalloidin (F-actin; red in merge) and presynaptic terminals labeled with synaptotagmin (ST; blue in merge). Close apposition between postsynaptic F-actin accumulations and presynaptic terminals is observed (panels 1 and 2). (B) DiI (green in merge)-labeled neurons were incubated with 5 or 55 mM KCl before fixation and labeled with phalloidin (blue in merge). The F-actin accumulations on the dendritic surface coincide with the membranous protrusions detected with DiI (5 mM KCl; arrowheads). Upon 55 mM KCl treatment (55 mM KCl), DiI and F-actin labeling reveal the absence of actin-rich membranous protrusions and a rather high accumulation of F-actin in the dendritic shaft compared with controls (5 mM KCl). (C) Immunofluorescence analysis of hippocampal neurons treated with 5 or 55mM KCl before fixation. Untreated and control buffer-treated (5 mM KCl) cells show similar numbers of dendritic spines, whereas 55 mM KCl-treated neurons exhibit an 85% reduction of dendritic spine number as judged by F-actin–rich protrusions at the surface (graph a). Replacing neurons into growth medium (55 mM KCl + wash) allowed a nearly complete recovery of spine number (graph b). Error bars represent SD. ***, $P < 0.001$; one-way ANOVA followed by Tukey's post-hoc test. Bars, 5 μm.

restrictive control over membrane-signaling events could be involved in the expansion/retraction of dendritic spines upon synaptic stimulation. In support of this, in cultured hippocampal neurons, activation of AMPA and *N*-methyl-D-asparate (NMDA) receptors (NMDARs) results in dendritic spine collapse in an actin-dependent manner (Halpain et al., 1998; Hering and Sheng, 2003). Furthermore, manipulation of Rho GTPase activity via the expression of constitutively active or dominant-negative mutants affects dendritic spine number and shape (for review see Dillon and Goda, 2004). In *Xenopus laevis* optic tectal neurons, the stimulation of glutamate receptors (GluRs) lowers RhoA activity (Li et al., 2002). However, many questions remain open: how do these three locally restricted events—membrane receptor activation, modulation of RhoA activity, and actin dynamics—relate mechanistically? How does the activation of excitatory neurotransmitter receptors influence the activity of RhoA in spines? What are the molecular mechanisms controlling the underlying actin cytoskeleton? To address these issues, we performed a series of cell biological approaches in embryonic rat hippocampal neurons in culture during the time of ongoing excitatory synaptic activity.

Results

Our first goal was to reproduce the experimental conditions that would allow us to visualize dendritic spine dynamics in cultured hippocampal neurons, a system extensively used to study dendritic spines (Fischer et al., 1998; Korkotian and Segal, 2001a,b). Staining of mature hippocampal neurons with labeled phalloidin readily revealed actin-rich structures along the dendritic shaft (Fig. 1 A). Magnification of dendritic areas allowed us to observe individual actin clusters projecting away from the dendritic shaft (Fig. 1 A, panels 1 and 2). Approximately 97% of these actin protuberances exhibited presynaptic terminals in their direct vicinity (as seen by synaptotagmin [ST] labeling). Labeling live cells with the lipophilic probe DiI confirmed that such actin accumulations label membranous projections emerging from the dendritic surface (Fig. 1 B). Furthermore, incubation with elevated levels of potassium ions (55 mM KCl), which are known to induce neurotransmitter release (Corder et al., 1982; Waring et al., 1999; Chen and Lang, 2003), led to a drastic simplification of the dendritic surface and induced major rearrangements of the underlying actin cytoskeleton (Fig. 1 B). Statistical analysis showed that stimulated cells exhibited a significant 85% reduction in dendritic actin-based projections in comparison with untreated or control buffer–treated cells (5 mM KCl; Fig. 1 C, graphs). The specificity of the aforementioned effects was demonstrated by recovery of the number of filamentous actin (F-actin)–rich projections back to control-like values when 55 mM KCl medium was replaced with normal growth medium (Fig. 1 C, 55 mM KCl + wash). Phenotypically, the surface retraction of actin-rich spines upon 55 mM KCl treatment was associated with a dramatic increase of actin filaments within the dendritic shaft (Fig. 1 C, 55 mM KCl; and Fig. S1, available at http://www.jcb.org/cgi/content/full/jcb.200506136/DC1). Because similar effects are induced by the addition of the neurotransmitters AMPA and NMDA (see Fig. 4), this first series of results established the basis for attempting our next goal: to determine the possible mechanisms involved in architectural control of F-actin–rich dendritic spines.

RhoA regulates dendritic spine actin in a GluR-dependent manner

RhoA is an actin-regulatory protein that enriches in discrete structures along the dendritic surface in hippocampal neurons (Hall, 1998; Nakayama et al., 2000; Santos Da Silva et al., 2004). Therefore, we wondered whether the aforementioned 55 mM KCl-induced changes in spine number and actin remodeling involved the modification of RhoA activity. Western blot analysis of subcellular fractions obtained by biochemical fractionation of rat brain extracts revealed that RhoA is present in postsynaptic fractions (Fig. 2 A). To dissect the role of RhoA activity in dendritic spines, we immunolabeled control as well as 55 mM KCl-treated cultured hippocampal neurons for RhoA and F-actin and performed confocal microscopy. To exclusively visualize the active and, thus, membrane-bound RhoA, the cytosolic protein pool was detergent extracted from the cells. Analysis of confocal slice images demonstrated that under control conditions, apart from being present throughout the entire dendritic tree, a considerable amount of active RhoA clusters colocalized with the F-actin–rich dendritic spines (Fig. 2 B, panel 1). As expected, 55 mM KCl-treated neurons presented a drastically changed F-actin pattern in respect to controls: namely, the loss of actin-rich dendritic spines and accumulation of F-actin fibers in the shaft (Fig. 1, B and C). Concomitantly with the increased F-actin signal intensity, the amount of active RhoA in the dendritic shaft was largely enhanced (Fig. 2 B, panel 2 and graph). These data suggested that the 55 mM KCl-induced changes in the F-actin phenotype could possibly be induced via alterations in the levels of active RhoA. To test this hypothesis, we analyzed the amount of GTP-bound active RhoA in whole cells and in synaptosomes. Stimulation of synaptosomes with 55 mM KCl significantly reduced the levels of active RhoA in respect to control buffer treatment (Fig. 3 A). Such synaptic reduction of RhoA activity could explain the loss of actin-rich spines observed upon 55 mM KCl treatment (Fig. 1, B and C). On the other hand, stimulation of whole cells with 55 mM KCl greatly increased the amount of active RhoA (Fig. 3 A). Given the fact that in total cell extract the amount of extra synaptic material greatly exceeds the synaptic, the observed 55 mM KCl-triggered increase of RhoA activity most likely reflects extrasynaptic pools of RhoA, which, in turn, could explain the formation of actin cables along the dendritic shaft.

Thus, we sought to define whether such reduction of RhoA activity in synaptosomes and the drastically changed F-actin phenotype observed in cultured neurons are in fact triggered by activation of GluRs in the excitatory postsynapse rather than being secondary effects of the treatment. For this, synaptosomes were preincubated with the NMDA- and AMPA-type GluR antagonists MK-801 and CNQX, respectively, and RhoA activity levels were measured biochemically (Fig. 3 B). Preincubation with MK-801 and CNQX prevented the 55 mM KCl-induced decrease of RhoA activity levels,which is consistent

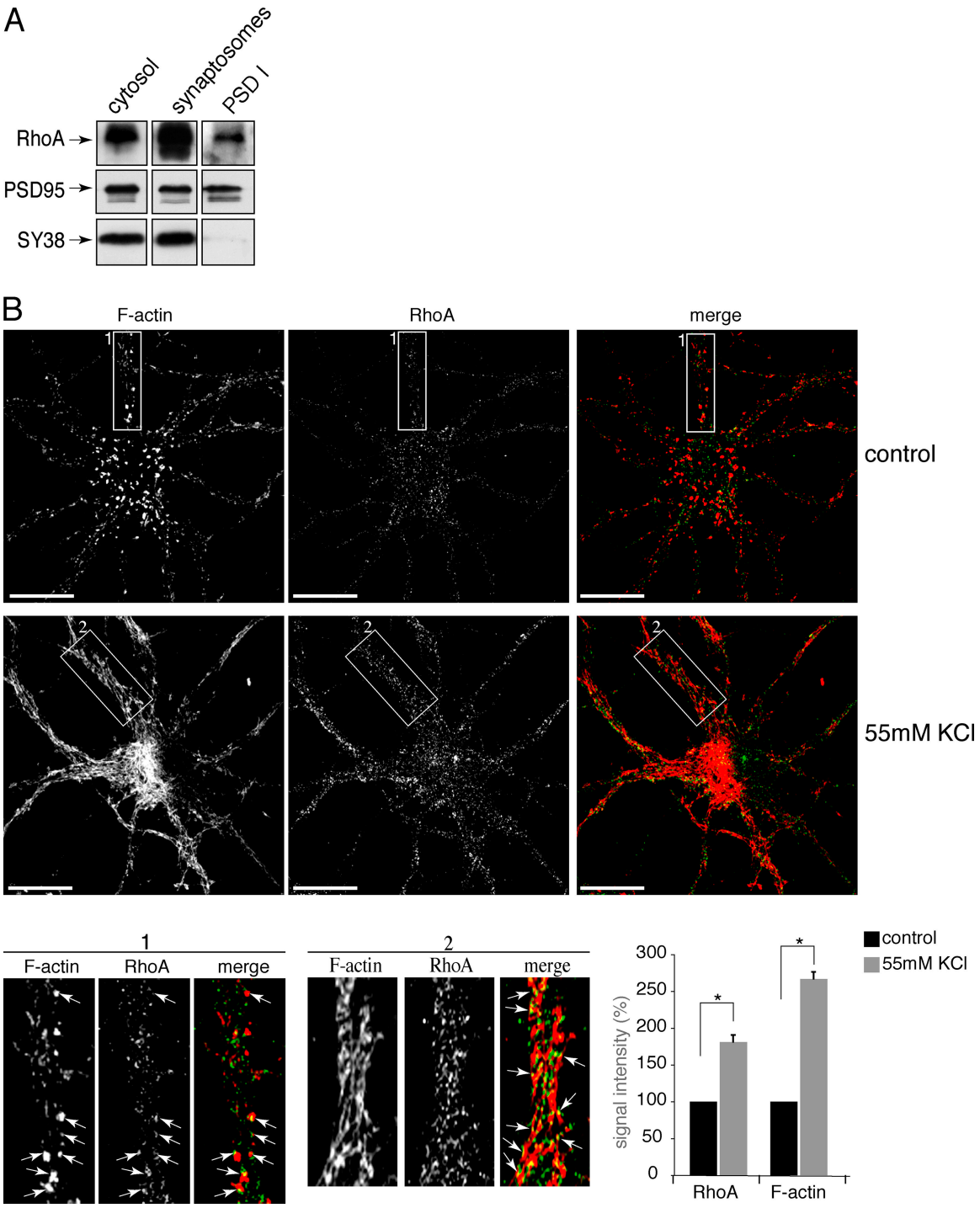

Figure 2. **RhoA and F-actin behave similarly upon 55 mM KCl treatment.** (A) RhoA is detectable in cytosol, synaptosomes, and in postsynaptic density fraction (PSD I). The enrichment of PSD 95 in respect to presynaptic protein synaptophysin demonstrates the pureness of the postsynaptic fraction. (B) Confocal slice of immunofluorescence analysis of RhoA localization to the dendritic spine. The cells were detergent extracted to visualize only membrane-bound and, thus, active RhoA. In untreated or control buffer–treated cells, RhoA localizes to the actin-rich domains of the cell (control). Enlargement of a dendritic segment revealed that apart from being present throughout the dendritic shaft, RhoA colocalizes with dendritic spine actin (panel 1, arrows). Note the 55 mM KCl-induced loss of dendritic spine actin and accumulation of F-actin cables in the shaft (55 mM KCl). In these cells, compared with controls, RhoA and F-actin signal intensity are greatly increased (graph). Error bars represent SD. The enlarged dendritic segment illustrates the colocalization between RhoA and F-actin in the dendritic shaft (panel 2; arrows indicate regions of colocalization). RhoA is green and F-actin is red in merged images. *, $P < 0.001$; paired *t* test. Bars, 10 μm.

with the aforementioned effects being caused by excessive neurotransmitter release (Fig. 3 B). Moreover, preincubation of cultured neurons with either antagonist prevented the 55 mM KCl-induced loss of F-actin– rich dendritic spines as well as the formation of actin cables in the dendritic shaft (Fig. 3 C, graph). This illustrates that although we cannot exclude the

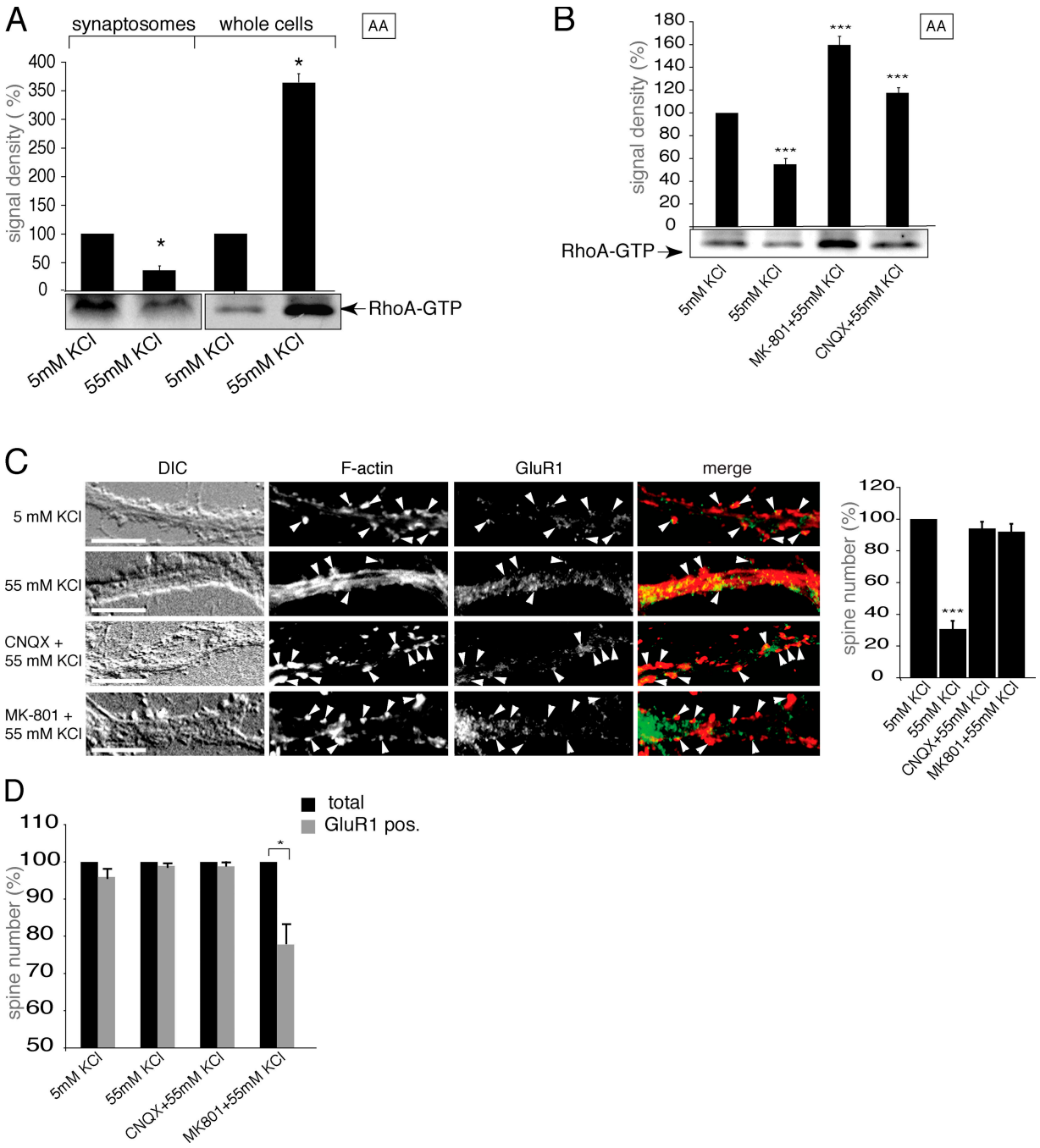

Figure 3. **RhoA activity in synaptosomes is reduced upon 55 mM KCl treatment in a GluR-dependent manner.** (A) Active RhoA (RhoA-GTP) was isolated from synaptosomes and whole cell extracts using a RhoA activation assay (AA). 55 mM KCl significantly decreased RhoA activity in synaptosomes compared with control buffer treatment (5 mM KCl). On the other hand, treatment of whole cells with 55 mM KCl largely increased RhoA activity in respect to controls. (B) Activation assay. Preincubation with MK-801 and CNQX prevented the 55 mM KCl-induced decrease of synaptosomal RhoA activity. (C) Dendritic segments showing GluR1 localization in mature neurons. In control cells, GluR1 labeling (green in merge) was punctate, and the protein colocalized with F-actin (red in merge)–rich dendritic spines (5 mM KCl, arrowheads). Upon 55 mM KCl treatment, F-actin cables formed in the shaft, and spine number was reduced (55 mM KCl, graph). Preincubation with CNQX or MK-801 prevented the spine loss and the formation of actin cables (graph). (D) Graph showing total spine number versus the number of spines containing GluR1 labeling. In cells treated with 5 and 55 KCl or CNQX + 55 mM KCl, the percentages were comparable (96–100%), whereas MK-801 + 55 mM KCl led to a 30% reduction of GluR1-containing spines (white arrowheads in C indicate GluR1-positive spines). Error bars represent SD. *, $P < 0.001$; paired *t* test. ***, $P < 0.001$; one-way ANOVA followed by Tukey's multiple comparison test. Bars, 5 μm.

participation of presynaptic RhoA pools under these conditions (Wang et al., 2005), the observed 55 mM KCl-induced changes in synaptic RhoA activity and F-actin are mainly caused by modulation of postsynaptic RhoA. Analysis of the subcellular localization of GluR1 in mature hippocampal neurons provided further evidence that neurotransmitter-mediated 55 mM KCl-induced synaptic changes are caused by the activation of GluRs. In control cells under control conditions, GluR1 labeling was very punctate and mainly restricted to dendritic spines but was largely absent from the dendritic shaft (Fig. 3 C, 5 mM KCl).

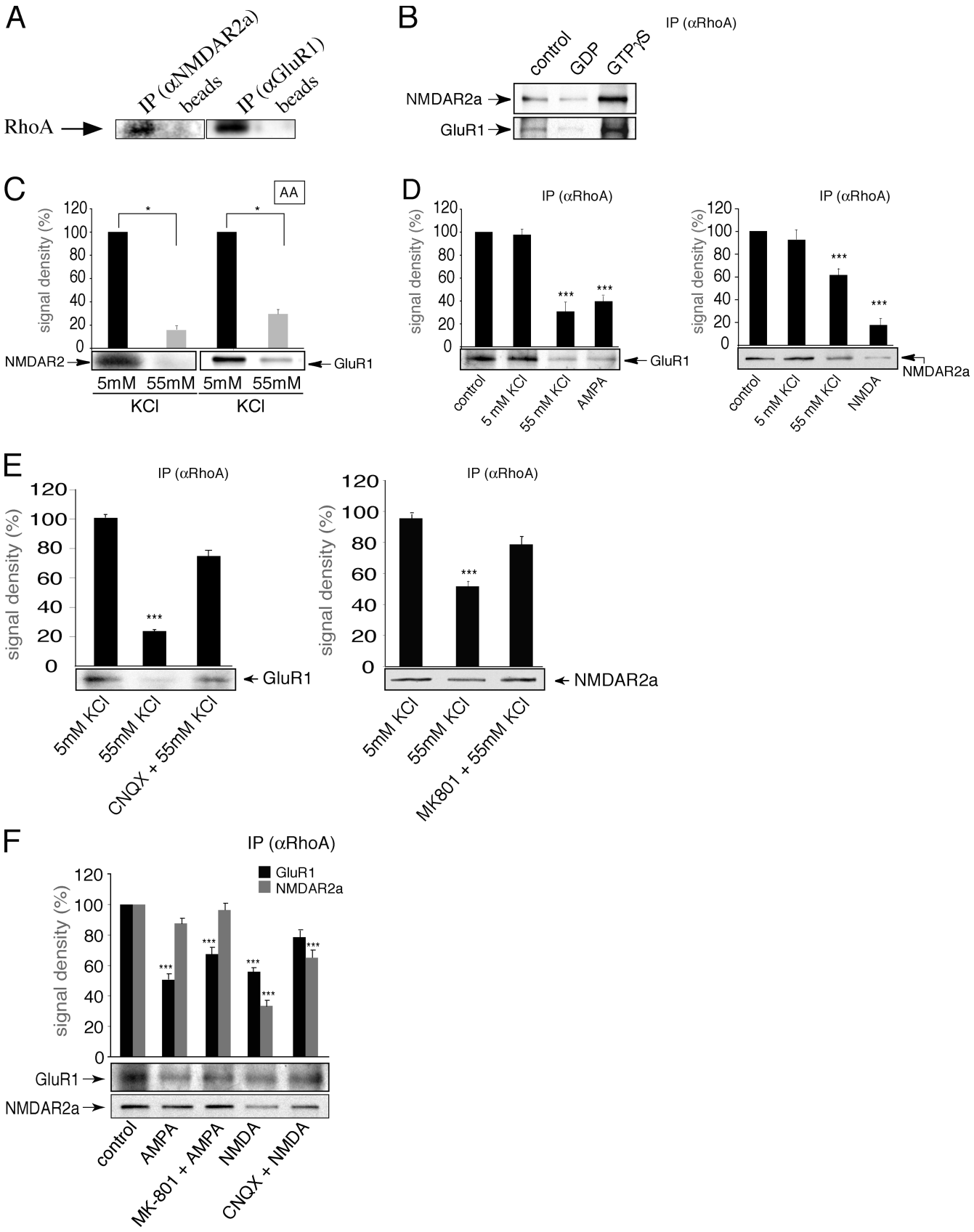

Figure 4. **Activity of iGluRs determines the amount of receptor interaction with RhoA.** (A) RhoA was coprecipitated with NMDAR2a and GluR1, respectively, from synaptosomal preparations. (B) Immunoprecipitation of RhoA from synaptosomes. The spine resident membrane proteins NMDA receptor 2a (NMDAR2a) and glutamate receptor 1 (GluR1) coprecipitate with RhoA. Incubation with GTPγS before the immunoprecipitation increased the interacttions to RhoA, whereas preincubation with GDP had the opposite effect. (C) RhoA activation assay. Reduced RhoA activity upon high potassium treatment

Upon 55 mM KCl treatment, the protein distribution became more diffuse, and large amounts of GluR1 localized to the dendritic shaft (Fig. 3 C, 55 mM KCl). Preincubation with CNQX prevented the displacement of GluR1 into the shaft, and the punctate staining largely colocalized with dendritic spines, similar to controls (Fig. 3 C, CNQX + 55 mM KCl). A similar, although less effective, protection was achieved with the NMDAR antagonist MK-801 (Fig. 3 C, MK-801 + 55 mM KCl). Although in MK-801–pretreated cells total spine number was similar to controls, in some areas of the cell the labeling of GluR1 appeared slightly less punctate.

To further examine GluR1 localization to dendritic spines under the different experimental conditions, we considered the total amount of F-actin–rich dendritic spines as 100% and compared this with the number of spines actually containing GluR1 (Fig. 3 E). We found that in 5 mM KCl, 55 mM KCl, and CNQX + 55 mM KCl-treated neurons, nearly 100% of all spines contained GluR1 labeling (Fig. 3 E). Neurons treated with MK-801 before 55 mM KCl incubation exhibited a significant 25% decrease of GluR1-positive, F-actin–rich spines. As we did not exclusively label plasma membrane GluR1, we can only speculate about the nature of such altered GluR1 pattern. However, we believe that the 55 mM KCl-induced partial displacement of GluR1 from the synapse into the shaft could be caused by receptor endocytosis and recycling as a response to altered synaptic activity (Ehlers, 2000). This, in turn, could explain the observed decrease of GluR1-positive spines and the increase of shaft GluR1. Collectively, these data suggest that the 55 mM KCl-induced modulation of synaptic RhoA activity and, thus, local F-actin stability directly depend on the activity of excitatory neurotransmitter rather than result from a generalized entry of Ca^{2+} induced by such treatment. The data also suggest that activation of both receptor types is necessary to induce depolymerization of dendritic spine actin.

RhoA interacts with NMDA- and AMPA-type GluRs in an activity-dependent manner

Given the aforementioned findings and considering that the activation of RhoA and, thus, its capacity to favor actin polymerization depends on the degree of its association to membranes (Leung et al., 1995; Matsui et al., 1996), we reasoned that its role in spine stability might be instructed via immediate signaling from membrane components of the transmission machinery. In fact, we found that RhoA coprecipitated with NMDAR2a and GluR1 from synaptosomal preparations (Fig. 4 A; for mock experiments see Fig. S2, available at http://www.jcb.org/cgi/content/full/jcb.200506136). Vice versa, we performed coimmunoprecipitation with RhoA antibody and found that GluR1 and NMDAR2a coimmunoprecipitated with RhoA preferentially in its active state (Fig. 4 B, GTPγS vs. GDP treatment). Thus, we hypothesized that the reduction of RhoA activity observed upon 55 mM KCl treatment (Fig. 2 C) could be caused by signaling from NMDAR2a and GluR1. In fact, the amount of both receptors coprecipitating with active RhoA was largely reduced after 55 mM KCl (Fig. 4 C). To examine the relationship between RhoA and excitatory neurotransmitter receptors more thoroughly, synaptosomal preparations were stimulated with 55 mM KCl, AMPA, or NMDA, and the efficiency of the RhoA receptor interaction was measured biochemically. In all cases, the interaction of RhoA with NMDAR2a and GluR1, respectively, was significantly decreased (Fig. 4 D). Furthermore, incubation of synaptosomal preparations with NMDA and AMPA receptor antagonists MK-801 and CNQX prevented the 55 mM KCl-induced detachment between RhoA and NMDAR2a or GluR1, respectively (Fig. 4 E). Importantly, stimulation with AMPA led to a reduction of NMDAR2a–RhoA interaction levels, and, similarly, NMDA induced detachment of GluR1 and RhoA (Fig. 4 F). This could be prevented by preincubation of the respective antagonists before stimulation, meaning MK-801 for NMDAR2a–RhoA and CNQX for GluR1–RhoA binding (Fig. 4 F). This suggests that cross talk between AMPA and NMDARs exists, meaning that stimulation of one receptor type leads to indirect activation of the other and, as such, reflects on the reduced RhoA receptor interaction we observed here. Summarizing, these data demonstrate the existence of an ionotropic GluR (iGluR)–mediated RhoA-dependent signaling pathway that directly controls dendritic spine F-actin stability.

Association of RhoA to mGluR1 depends on AMPA-type GluR activity and is independent of RhoA activity levels

We next investigated whether the interaction of RhoA with neurotransmitter receptors was restricted to iGluRs only. We found that metabotropic GluR1 (mGluR1), which is closely associated to the excitatory postsynaptic density (PSD; Mateos et al., 2000), coprecipitated with RhoA from synaptosomal preparations (Fig. 5 A). The specificity of the interaction was confirmed by performing the reverse immunoprecipitation using mGluR1 antibody for coprecipitating RhoA from synaptosomes (Fig. 5 B). However, unlike NMDAR2a and iGluR1, the interaction between RhoA and mGluR1 was not reduced upon stimulation with 55 mM KCl, AMPA, or NMDA (Fig. 5 A). On the contrary, the amount of mGluR1 that coprecipitated with RhoA from synaptosomes was greatly increased by this

(Fig. 3 A) diminishes coprecipitation of NMDAR2 and GluR1 with active RhoA (graph). *, $P < 0.001$; paired *t* test. (D) Less GluR1 and NMDAR2a coimmunoprecipitate with RhoA in synaptosomes after 55 mM KCl compared with control- (graph) or 5 mM KCl-treated samples. Similar effects are observed after direct stimulation with AMPA or NMDA, respectively. (E) Preincubation with specific antagonists for NMDA and GluRs MK-801 and CNQX, respectively, prevented the decrease of RhoA–GluR interaction induced by 55 mM KCl. (F) Biochemical analysis of the cross reactivity between GluR1 and NMDAR2a. Preincubation with NMDA antagonist MK-801 partially prevented the AMPA-induced reduction of GluR1–RhoA interaction (compare AMPA with MK-801 + AMPA). Furthermore, direct stimulation with NMDA decreased the amount of GluR1–RhoA interaction, and this could partially be blocked by CNQX (compare NMDA with CNQX + NMDA). On the other hand, stimulation with AMPA lowered RhoA–NMDAR2a interaction levels and, as such, could be prevented by preincubation with MK-801. Error bars represent SD. ***, $P < 0.001$; one-way ANOVA followed by Tukey's multiple comparison tests.

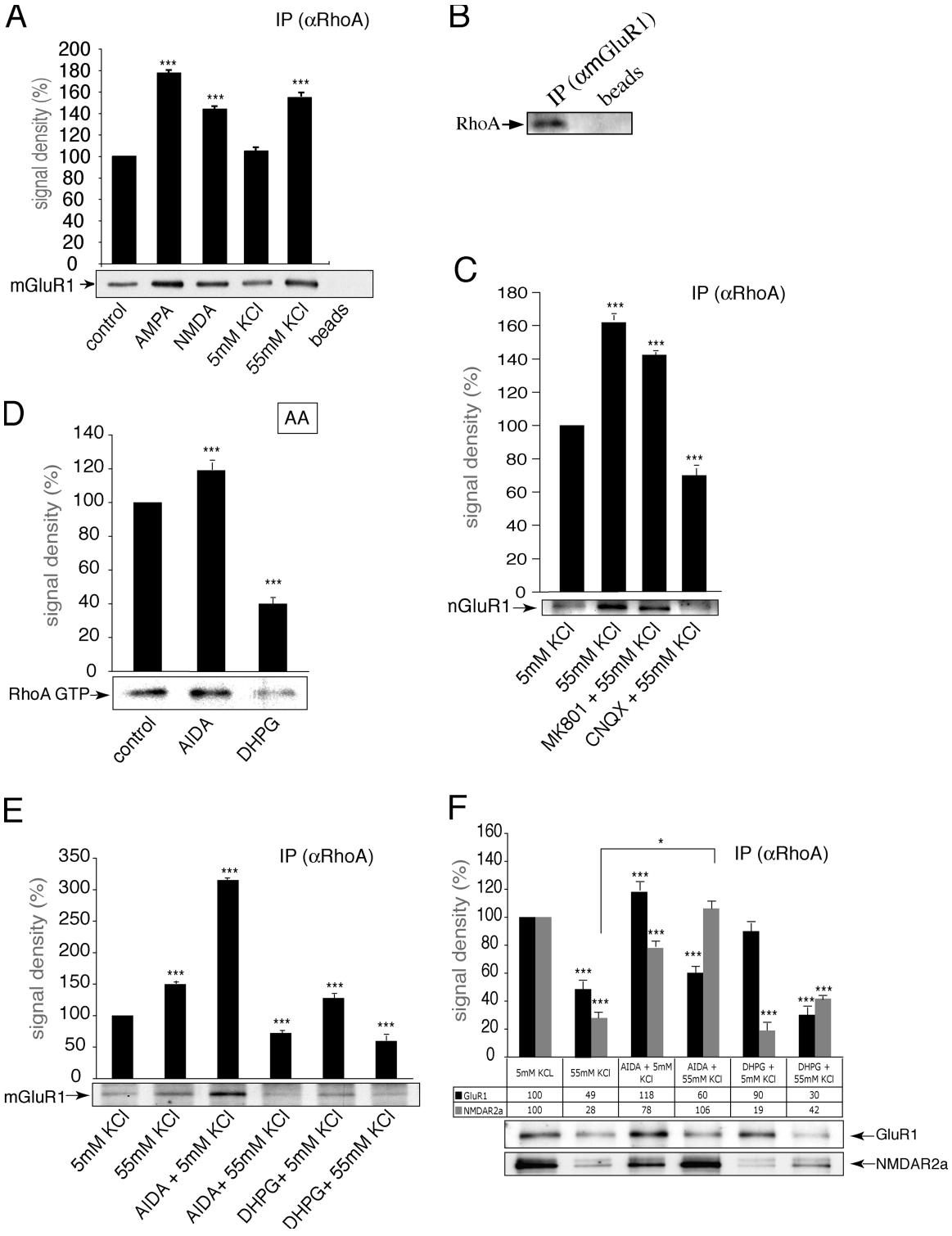

Figure 5. **Association of RhoA with mGluR1 depends on AMPA receptor activation and is independent of RhoA activity levels.** (A) mGluR1 coprecipitates with RhoA from rat synaptosomal preparations. Stimulation with AMPA, NMDA, or 55 mM KCl increased the interaction of mGluR1with RhoA. (B) Immunoprecipitation of mGluR1 from synaptosomes leads to coprecipitation of RhoA. (C) CNQX but not MK-801 prevents the 55 mM KCl-induced amplification of RhoA–mGluR1 interaction. (D) Activation assay performed on synaptosomes. Incubation with mGluR1 antagonist (AIDA) increases RhoA activity, whereas the agonist (DHPG) lowers activity levels of RhoA. (E) Effect of AIDA and DHPG on RhoA affinity to mGluR1. In respect to controls (5 mM KCl), incubation of synaptosomes with AIDA (AIDA + 5 mM KCl) and DHPG (DHPG + 5 mM KCl) increases the amount of receptor–RhoA interaction. Although the effect of AIDA appears very drastic, DHPG only slightly increases the RhoA–mGluR1 interaction. In both cases (AIDA and DHPG), subsequent treatment with 55 mM KCl leads to the opposite effect, inducing a drastic reduction of RhoA–mGluR1 interaction levels (AIDA + 55 mM KCl and DHPG + 55 mM KCl). (F) Effect of mGluR1 activity on AMPA and NMDAR interaction with RhoA. RhoA–GluR1 interaction was slightly (118%) increased by AIDA (AIDA + 5 mM KCl). DHPG did not have any significant effect (DHPG + 5 mM KCl). In both cases, stimulation with 55 mM KCl led to a detachment between RhoA and GluR1 (compare AIDA + 55 mM KCl and DHPG + 55 mM KCl with 55 mM KCl). AIDA slightly decreased the amount of NMDAR2a precipitating with RhoA under control conditions (compare AIDA + 5 mM KCl with 5 mM KCl). NMDAR2a resisted the 55-mM KCl stimulus in AIDA-treated samples, as

treatment (Fig. 5 A). To scrutinize the relationship between iGluRs and mGluRs, we incubated synaptosomes with MK-801 and CNQX before 55 mM KCl treatment and analyzed the amount of mGluR1–RhoA interaction (Fig. 5 C). We found that CNQX alone but not MK-801 blocks the increased interaction of RhoA with mGluR1 caused by 55 mM KCl (Fig. 5 C), indicating that activation of AMPA, rather than NMDARs, is necessary to allow RhoA to change interaction partners (i.e., detaching from iGluRs while gaining affinity to mGluRs). Overall, the detachment from iGluRs appears to result simply from conformational changes, as RhoA interaction with GluR1 and/or NMDAR2a decreases or increases according to their activity state. The more active the receptor, the less its affinity for active RhoA and, therefore, the more instable the surrounding actin network. Although not tested here, the observed changes in RhoA interaction partners, provoked by excitatory stimuli (namely 55 mM KCl, NMDA, and AMPA) may lead to the stabilization of mGluRs at the plasma membrane, which, in turn, could relate to the selective endocytosis and recycling of iGluRs.

To better understand the relationship between mGluR1 signaling and synaptic RhoA activity, we treated synaptosomes with AIDA and with DHPG, an mGluR type I–specific antagonist and agonist, respectively. We found that activity levels of mGluR1 affected the levels of synaptic RhoA activity, as AIDA led to an increase of RhoA activity, whereas DHPG had the opposite effect (Fig. 5 D, graph). This, in turn, affected the amount of interaction between RhoA and mGluR1 (Fig. 5 E). Incubation with AIDA (AIDA + 5 mM KCl) drastically increased the amount of mGluR1–RhoA interaction, whereas DHPG (DHPG + 5 mM KCl) did not have a significant effect in respect to controls (Fig. 5 E, compare with 5 mM KCl). Furthermore, we found that incubation with both AIDA and DHPG, followed by 55 mM KCl, blocked the increased association of RhoA to mGluR1 (Fig. 5 E, compare AIDA + 55 mM KCl and DHPG + 55 mM KCl with 55 mM KCl alone). However, although direct inhibition of mGluR1 increases the amount of active RhoA (Fig. 5 D) and the amount of mGluR1–RhoA interaction, respectively (Fig. 5 E), we cannot assume that the 55 mM KCl-induced enhanced interaction with RhoA is caused by the simple inactivation of mGluR1, as blockage of this G protein–coupled receptor in either state via incubation with its specific agonist (DHPG) or antagonist (AIDA) before 55 mM KCl treatment led to a decreased interaction with RhoA (in contrary to simple 55 mM KCl incubation; Fig. 5 E). These data demonstrate that although activity levels of mGluR1, similar to iGluRs, locally affect RhoA activity levels, the observed enhanced RhoA affinity for mGluR1 under 55 mM KCl treatment is independent of RhoA activity levels (as 55 mM KCl lowers RhoA activity) and is determined by two major components: (1) the activation of AMPA receptors (as blockage with CNQX prevents the association of RhoA to mGluR1 upon 55 mM KCl); and (2) the cycling of mGluR1 between its active and inactive state.

Considering these data, we were curious to investigate whether activity of mGluR1 affected the interaction between iGluRs and RhoA. For this, we incubated synaptosomes with AIDA and DHPG, subsequently added 55 mM KCl, and analyzed the various RhoA receptor interactions biochemically (Fig. 5 F). As previously described, stimulation with 55 mM KCl lowered the amount of GluR1/NMDAR2a–RhoA interaction noticeably (Fig. 5 F, compare 5 mM KCl with 55 mM KCl). Preincubation with AIDA slightly increased GluR1–RhoA interaction levels (118%), whereas DHPG did not significantly affect the amount of RhoA receptor interaction (Fig. 5 F, black bars; compare 5 mM KCl with AIDA/DHPG + 5 mM KCl). However, in both cases, 55 mM KCl led to RhoA–GluR1 interaction levels similar to controls (compare 55 mM KCl with AIDA/DHPG + 55 mM KCl). NMDAR2a, on the other hand, was sensitive to the AIDA and DHPG treatment (Fig. 5 F, gray bars). Inhibition of mGluR1 prevented the 55 mM KCl-induced detachment between NMDAR2a and RhoA (AIDA + 55 mM KCl). Simple activation of mGluR1, on the other hand, led to a drastic reduction of NMDAR2a–RhoA interaction levels, similar to what was normally observed upon 55 mM KCl treatment (DHPG + 5 mM KCl). Subsequent stimulation of DHPG-treated samples with 55 mM KCl did not have a significant effect on NMDAR2a–RhoA interaction levels, as they remained low (DHPG + 55 mM KCl).

Summarizing these data and the previously discussed results, we conclude that in excitatory synapses, activation of AMPA-type GluRs directly affects type I mGluRs, thus increasing mGluR1 affinity to RhoA. This could lead to stabilization of the receptor at the plasma membrane so as to allow for specific mGluR1-mediated signaling events necessary for different neurotransmission-induced events. In fact, we demonstrated that activation of mGluR1 before 55 mM KCl stimulation decreased NMDAR but not AMPA receptor response. To analyze in further detail the relationship between ionotropic and metabotropic receptors, we performed double treatments, preincubating synaptosomes with both MK-801 + AIDA or MK-801 + DHPG before 55 mM KCl and analyzed the amount of mGluR1 coprecipitating with RhoA. Unfortunately, the incubation of synaptosomes with two agonists/antagonists at the same time led to inconsistent information. Yet, some of them clearly indicated that combined incubations (MK-801 + AIDA/DHPG or CNQX + AIDA/DHPG) did not prevent the detachment between mGluR1 and RhoA, provoked by AIDA/DHPG + 55 mM KCl [not depicted]). Although only preliminary, these data strengthen the notion that the 55 mM KCl-induced increase in the affinity between RhoA and mGluR1 requires AMPA receptor activity and also that such signaling can be overruled by direct modulation of mGluR1 activity levels, which, in turn, modulates NMDAR response.

NMDAR2a–RhoA interaction levels remained elevated (compare AIDA + 55 mM KCl and 55 mM KCl). Although simple DHPG treatment drastically reduced the amount of NMDAR2a–RhoA interaction (compare DHPG + 5 mM KCl and 5 mM KCl), subsequent incubation with 55 mM KCl led to interaction levels similar to controls (compare DHPG + 55 mM KCl and 55 mM KCl). Error bars represent SD. ***, $P < 0.001$; one way ANOVA followed by Tukey's multiple comparison tests. *, $P < 0.001$; paired *t* test.

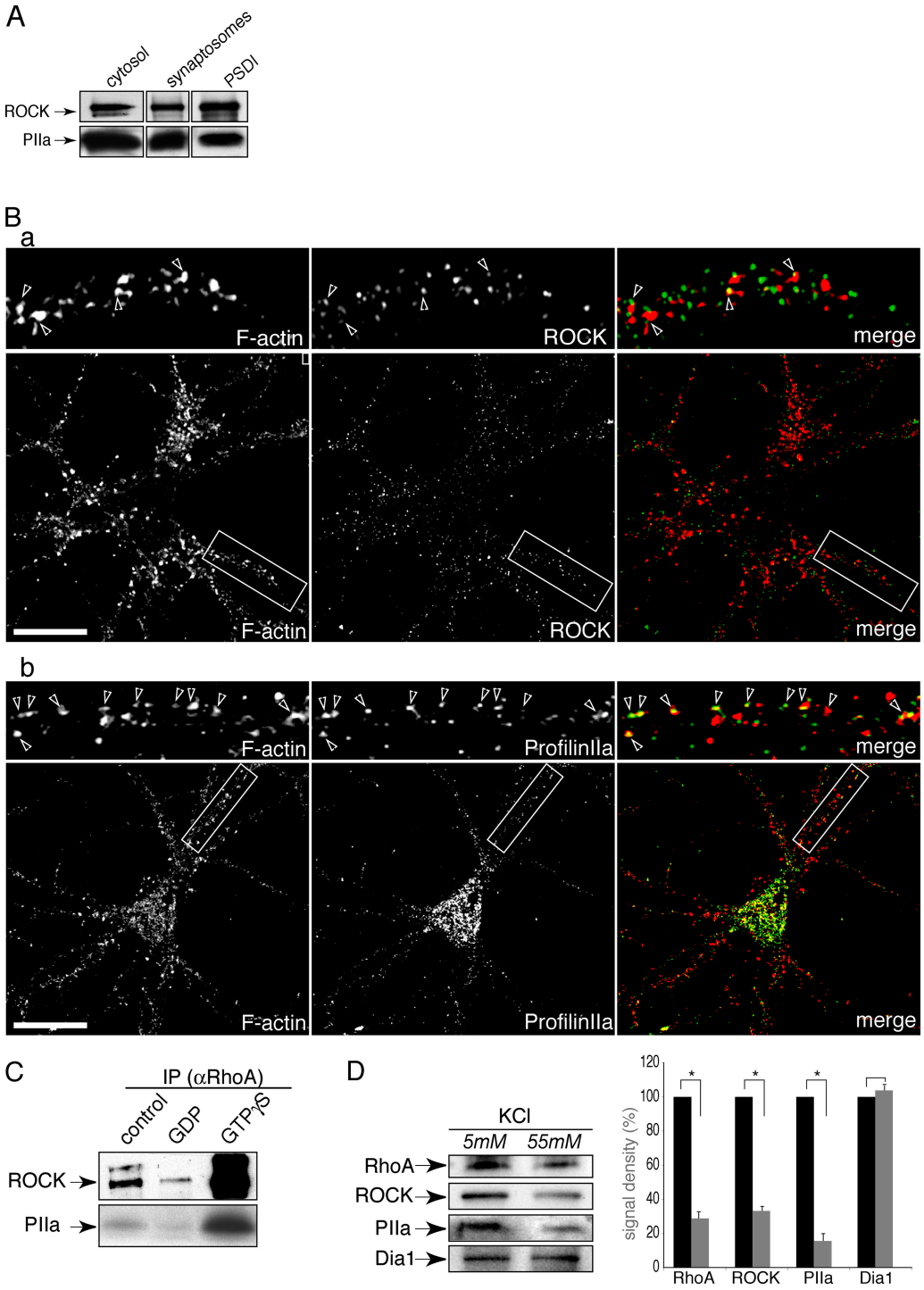

Figure 6. **RhoA-mediated dendritic spine F-actin stability is regulated in a ROCK–PIIa-dependent manner.** (A) Analysis of subcellular fractionation of adult rat brain showed that ROCK and PIIa are detectable in cytosol, synaptosomes, and in PSD I fractions. (B) Representative confocal slice images of mature hippocampal neurons labeled for ROCK (a; green in merge) and profilinIIa (PIIa, b; green in merge). Both proteins are present throughout the cell, preferentially in F-actin–rich regions (red in merge). Enlargement of dendritic segments revealed that apart from being present throughout the dendritic shaft, ROCK and PIIa colocalize with dendritic spine actin. Boxed areas in whole cell images mark the localization of enlarged dendritic segments shown in the figure. Arrowheads indicate points of colocalization between F-actin and ROCK or PIIa, respectively. (C) ROCK and PIIa both coimmunoprecipitate with RhoA from synaptosomal fractions, and such interaction is favored by RhoA activation (GTPγS) and reduced if RhoA is inactivated (GDP). (D) 55 mM KCl largely inactivates RhoA compared with control buffer–treated samples (5 mM KCl; see Fig. 2 C). Concomitantly, the amount of coprecipitated ROCK and PIIa with active RhoA (RhoA-GTP) is drastically reduced, whereas the quantity of coprecipitated Diaphanous (Dia1) is not altered. Error bars represent SD. *, $P < 0.001$; paired *t* test. Bars, 5 μm.

RhoA-mediated dendritic spine F-actin stability is regulated in a ROCK–ProfilinIIa-dependent manner

Our next aim was to understand how spine-associated RhoA forward neurotransmitter receptor derived information to the underlying actin cytoskeleton. RhoA-specific kinase (ROCK) and the neuronal-specific profilinIIa (PIIa) form a complex (ROCK–PIIa complex) that regulates (in a RhoA activity–dependent manner) local actin polymerization in the growth cones of young, unpolarized mammalian neurons as well as in the axon of polarized neurons (Da Silva et al., 2003, 2005). Thus, we investigated whether mature neurons possibly have the capacity to recruit this pathway to dendritic spines to locally regulate actin dynamics and, thus, synapse stability. The first indication for a possible involvement was the observation that the ROCK–PIIa complex is present in postsynaptic fractions purified from mature rat brain extracts (Fig. 6 A; for controls see Fig. 2 A). The localization in spines was confirmed by confocal microscopy of mature hippocampal neurons in culture (Fig. 6 B). Both proteins are present throughout the cell. Enlargement of dendritic segments showed that both proteins, apart from being present along the entire dendritic shaft, are also found in F-actin–rich dendritic spines. Therefore, we tested whether RhoA activity is necessary to efficiently recruit the ROCK–PIIa complex within spines. Both ROCK and PIIa precipitated with RhoA in synaptosomal extracts, and this interaction was favored by RhoA activation (Fig. 6 C). Because the latter depends on excitatory synaptic transmission (Figs. 2 and 3), we tested whether high KCl stimulation would reduce the formation of the RhoA-ROCK–PIIa complex in synaptosomes. Consistent with the previous data, the amount of ROCK and PIIa interacting with purified active RhoA was reduced upon high KCl stimulation (Fig. 6 D). Similar effects were obtained by direct stimulation with AMPA and NMDA (Fig. S3, available at http://www.jcb.org/cgi/content/full/jcb.200506136/DC1). To determine whether synaptic input restrictively modulates the activity of this particular set of RhoA-downstream players within dendritic spines, we analyzed the effect of 55 mM KCl on the interaction between RhoA and Diaphanous 1 (Dia1; Sahai and Marshall, 2002). The amount of Dia1 coprecipitating with active RhoA was not altered by high KCl treatment (Fig. 6 D), indicating that the interaction between RhoA and the ROCK–PIIa complex within the synapse is of a unique kind and reflects the functional importance of this signaling cascade for synaptic transmission–induced structural modifications.

Restrictive activation of caged ROCK inhibitor Y27632 induces localized spine retraction

We next set out to directly evaluate the importance of this pathway in the regulation of dendritic spines by locally inactivating RhoA–ROCK downstream signaling in a restricted dendritic segment while preserving its activity in the neighboring areas (Fig. 7). DiI-labeled mature neurons were incubated with a photosensitive ROCK inhibitor (caged Y27632). Local uncaging by stimulation with UV light induced local disruption of the activity of the ROCK–PIIa complex and was reflected by the rapid retraction of spines on the stimulated areas (Fig. 7 A). The neighboring dendritic segment, positioned outside of the pinhole during uncaging, did not show any noticeable alterations in spine structure (Fig. 7 B). Moreover, UV stimulation of dendritic segments of neurons treated with the vehicle buffer used to dissolve the caged compound did not induce changes in spines (Fig. 7 C). The dendritic spine retraction we observed under localized ROCK inactivation clearly demonstrates the involvement of this RhoA-dependent and ROCK–PIIa-mediated signaling cascade for stabilizing the actin cytoskeleton within spines.

Discussion

In this study, we illustrated that RhoA interacts with GluRs at the level of the PSD and regulates dendritic spine actin in a ROCK–PIIa-dependent manner. Such RhoA-dependent dendritic spine F-actin regulation is rapidly (within minutes) modulated in response to direct (AMPA and NMDA) or indirect (55 mM KCl) stimuli. Furthermore, we have managed to differentiate between iGluR and mGluR behavior to such stimuli and, moreover, dissected the differences between NMDA- and AMPA-type neurotransmitter receptors.

The role of iGluRs: differences in NMDA- and AMPA-type receptors

Generally, we found that the 55 mM KCl-induced reduction of dendritic spine F-actin stability and, consequently, the loss of excitatory synapses are triggered by an activity-dependent relationship between RhoA and iGluRs: the less active the receptors, the more interaction with RhoA and the higher, in turn, its GTPase activity level. Such a mechanism could provide the cell with a safe guard mechanism to guarantee a certain level of synaptic activity. If the amount of synaptic transmission is very low, the iGluRs will preferentially be inactive and will, via recruitment of RhoA, stabilize the underlying actin cytoskeleton to maintain or even enhance the stability of the postsynaptic structure. Therefore, this will enhance the possibility of excitatory transmission at this particular synapse. In the opposite situation, when excitatory stimulation occurs, the open/closed ratio and, thus, activity of iGluRs will increase, inducing a reduction of RhoA activity levels, which then allows loosening of the underlying actin cytoskeleton. Such reduced interaction with RhoA and the increased actin dynamics occurring at the PSD could give rise to many of the neurotransmission-induced mechanisms that have been observed: for example, the remodeling of spine shape and enhanced endocytosis and recycling of neurotransmitter receptors (Korkotian and Segal, 1999; Montgomery et al., 2005). However, despite their capacity to directly regulate postsynaptic actin stability, we found that AMPA and NMDAR signaling has differential effects on other neurotransmitter receptors at the excitatory PSD, namely mGluR1.

Type I mGluR signaling affects NMDA but not AMPA receptor response

Contrary to NMDAR2a and iGluR1, the interaction between RhoA and mGluR1 was greatly increased upon 55 mM KCl

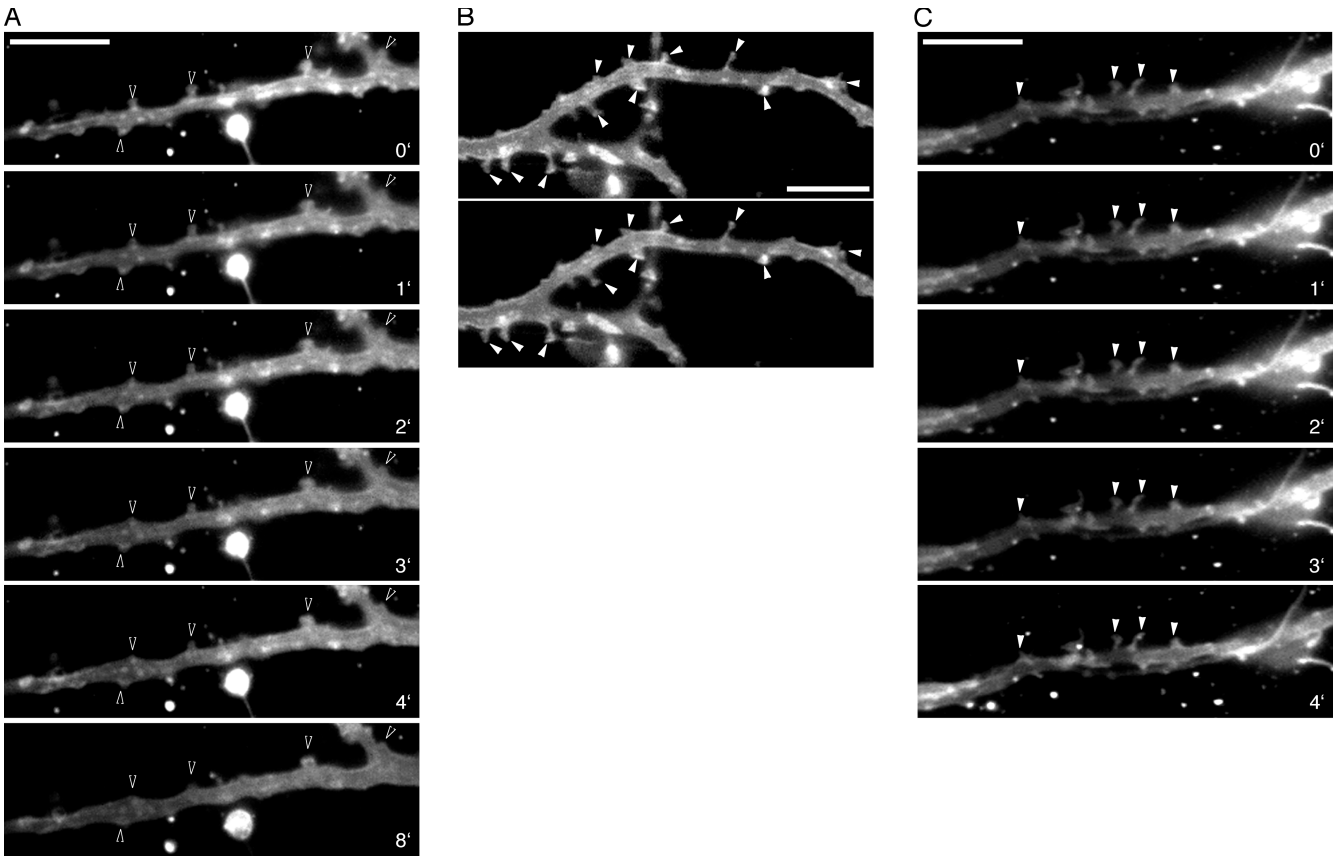

Figure 7. **Restrictive activation of caged ROCK inhibitor Y27632 induces localized spine retraction.** Single images of in vitro time-lapse experiments performed on DiI-labeled neurons incubated with caged ROCK inhibitor (caged Y27632). (A) Images of a dendritic segment (dendrite 1) before (top) and after (1–8 min) uncaging of Y27632 by exposure to UV light. Dendritic spines retract upon activation of the compound (arrowheads). (B) A neighboring dendrite located outside the pinhole during uncaging of dendrite 1. The spines on this dendrite remain stable and do not retract (arrow-heads). Compare top image (before uncaging of dendrite 1) with bottom image (after uncaging and observation of dendrite 1). (C) Dendritic segment of a DiI-labeled neuron treated with the vehicle buffer used to dissolve the caged compound. UV stimulation did not induce changes in spines. Compare top image with the four bottom images (arrowheads). Bars, 5 μm.

treatment. Interestingly, we found that such affinity mainly requires two conditions: the activation of AMPA receptors and the cycling of mGluR1 between its active and inactive state. Type I mGluRs have been implicated in a large variety of signaling events connected to different models of memory formation and have been shown to play important roles in various neuroprotective mechanisms (for review see Baskys and Blaabjerg, 2005). The increased interaction with RhoA observed upon 55 mM KCl could, therefore, allow mGluR1 to locally stabilize the underlying actin cytoskeleton to maintain its position at the plasma membrane. This, in turn, would allow for mGluR1-dependent signaling events to occur (e.g., the down-regulation of NMDAR response to avoid NMDA toxicity; Blaabjerg et al., 2003). In fact, we observed that altered mGluR1 activity has a direct effect on NMDAR2a response, as inactivation of this G protein–coupled receptor before treatment with 55 mM KCl reduced the NMDAR2a response to the stimulus, and the RhoA receptor interaction resisted the treatment. Direct activation of mGluR1, on the other hand, strongly reduced the affinity of NMDAR2a for RhoA. This, in turn, could have multiple effects on the stability of NMDARs at the PSD. As pointed out previously, the range of mGluR1-dependent signaling events is very wide, and we can only speculate about the exact biochemical mechanisms used to modulate NMDAR response (see respective model in Fig. 8). However, as incubation times were rather short (3 min) and all immunoprecipitation experiments were performed on synaptosomal preparations, we consider two possibilities as the most plausible: (1) modification of the intracellular calcium stores leads to an NMDAR insensitivity (because of its chemical properties as a calcium ion channel) while leaving AMPA receptor response mainly unmodified (AMPA receptors being mainly permeable for sodium ions); and (2) phosphorylation of the intracellular domain of NMDAR2a induces insensitivity of the receptor and, therefore, reduces its reaction to the treatment.

To summarize, this work illustrates in detail a signaling pathway by which neurotransmission events occurring at the excitatory synapse directly trigger the necessary cytoskeletal rearrangements at these domains and describes how these, in turn, modulate the response of the postsynapse. Certainly, one should address many more points to further understand the uniqueness of each neurotransmitter receptor and its signaling properties to the underlying actin cytoskeleton, yet we limited this study to three different receptor types to allow a more detailed analysis of the matter.

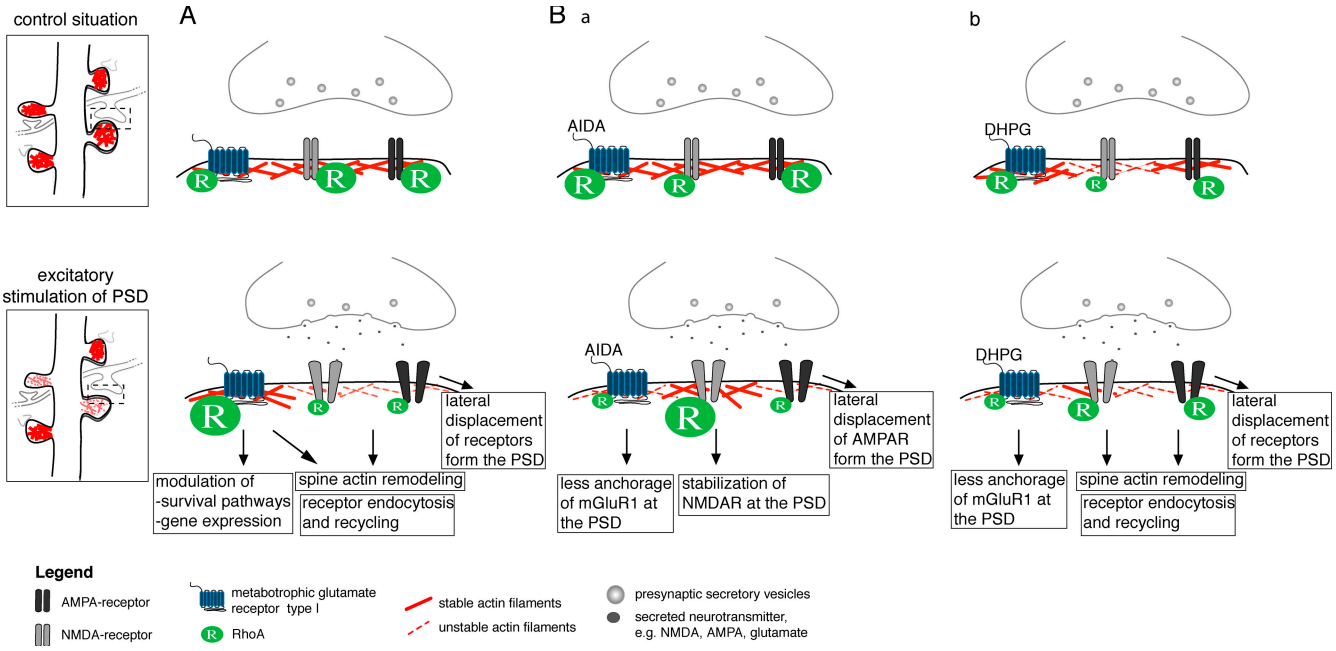

Figure 8. **Model describing the differential RhoA-related behavior of GluRs in response to excitatory stimuli.** (A) Under steady-state conditions, active RhoA interacts with all three neurotransmitter receptor types at the level of the excitatory PSD, thus stabilizing spine actin filaments via its downstream effector complex ROCK–PIIa (here referred to as RhoA for simplification). Stimulation of neurotransmitter receptors at the excitatory PSD reduces the amount of total synaptic RhoA activity and leads to the redistribution of RhoA interactions away from iGluR toward mGluRs. This leads to a localized destabilization of dendritic spine actin, consequently allowing for actin-based plasticity and the instability of iGluRs at the PSD. This, in turn, would allow for the regulation of excitability of the synapse via either endocytosis and recycling of iGluRs, possibly induced by mGluR1 signaling, or the lateral movement of the receptors away from the PSD. Moreover, the stabilization of mGluR1 at the plasma membrane could guarantee signaling events, which are necessary for the cell to adjust to the incoming stimuli, such as the regulation of gene expression and modulation of cell survival pathways. Dashed boxes in both the control situation and excitatory stimulation of PSD panels represent localization of the excitatory synapse illustrated in A, B1, and B2. (B) Model illustrating how mGluR1 modulates NMDAR response to excitatory stimuli. (B1) Without active mGluR1 present, NMDARs become immune to incoming excitatory stimuli. Upon stimulation, high amounts of RhoA remain attached to the receptor, possibly leading to the retention of this receptor at the PSD. (B2) Activation of mGluR1 with DHPG has the opposite effect. The amount of RhoA–NMDAR interaction is greatly reduced and most likely leads to destabilization of NMDAR at the excitatory PSD, consequently reducing NMDA excitability.

Materials and methods

Cell culture

Primary cultures of rat embryonic hippocampal neurons were prepared as described previously (Goslin and Banker, 1991). For biochemical analysis, 150,000 cells were plated per 30-mm plastic dish coated with 0.1 mg/ml poly-L-lysine. For morphological analysis, 100,000 cells were plated per 60-mm dish, each with six poly-L-lysine–coated glass coverslips, and for in vitro time-laps observations, the cells were plated on 40-mm poly-L-lysine–coated glass coverslips. All times referred to in the text and figure legends are after seeding (time of plating is 0 h). Y27632 was used at 24 nmol/ml (Calbiochem). Optionally, neurons were incubated with 1 μM MK-801 (Sigma-Aldrich) or 2 μM CNQX (Qbiogene) for 10 min before high potassium treatment (see below).

Antibodies

The following antibodies were used: mouse monoclonal anti-RhoA (26C4; Santa Cruz Biotechnology, Inc.), mouse monoclonal anti-ROCK (clone 21; BD Transduction Laboratories), mouse monoclonal anti-PSD95 (Upstate Biotechnology), mouse monoclonal antisynaptophysin (Boehringer), rabbit polyclonal anti–α-synuclein (a gift from C. Sanchez, Centro Biologia Molecular, Madrid, Spain), rabbit polyclonal anti-mGluR1 (AB-1504; Chemicon), rabbit polyclonal anti-PIIa (a gift from W. Witke, European Molecular Biology Laboratory, Monterotondo, Italy), rabbit polyclonal anti-GluR type 1 (Upstate Biotechnology), rabbit polyclonal anti-NMDAR2a (AB1555P; Chemicon), rabbit polyclonal anti-ST (a gift from M. de Hoop, Aventis, Frankfurt, Germany), and goat polyclonal anti-Dia1 (V20; Santa Cruz Biotechnology, Inc.). Goat anti–rabbit and goat anti–mouse AlexaFluor350/488/568 (Invitrogen) and donkey anti–mouse, goat anti–rabbit, and donkey anti–goat HRP-conjugated antibodies (GE Healthcare) were used as secondary antibodies.

Immunofluorescence

Cells were fixed in PFA/SEM buffer (4% PFA, 0.12 M sucrose, 3 mM EGTA, and 2 mM $MgCl_2$ in PBS), quenched with 50 mM ammonium chloride, and extracted with 0.1% Triton X-100. Specific protein detection was performed using previously mentioned antibodies (see previous section), and F-actin was labeled with TRITC-conjugated phalloidin (Sigma-Aldrich). Optionally, cells were labeled with a lipophilic tracer (DiI; Invitrogen) to visualize the plasma membrane. For this, fixed cells were incubated with a 67-μg/ml working solution of DiI prepared in 1× PBS for 30 min at room temperature before mounting. For visualization of active RhoA only, cells were incubated with 0.1% Triton before fixation with PFA/SEM to extract all soluble protein forms. Cells were observed using a microscope (DMIRE2; Leica) equipped with 40, 63, and 100× objectives (Leica) and a digital camera (Q550; Leica), and images were captured using the Qfluoro software (Leica). Optionally, samples were analyzed in a confocal scanning microscope (LSM 5110; Carl Zeiss MicroImaging, Inc.) on a platform (Axiovert 100 M; Carl Zeiss MicroImaging, Inc.).

In vitro time lapse

For in vitro time-lapse experiments, the plasma membrane of mature hippocampal neurons was labeled with a lipophilic tracer (DiI; Invitrogen). In brief, cells were incubated for 1 min at 37°C with a 67-μg/ml working solution of DiI prepared in equilibrated growth medium. The cells were incubated in HBSS for 10 min under culture conditions, and time-laps recording was performed. For this, the cells were treated as described previously (Bradke and Dotti, 1997). In brief, cells were placed in a temperature-controlled FCS-2 long-term observation chamber (Bioptechs) and positioned on the stage of an inverted microscope equipped with 40, 63, and 100× objectives (Leica), and images were captured using the Qfluoro software (Leica). Pictures of chosen cells were taken in 1-min intervals. In some cases, the cells were incubated with a 2-μM solution of photosensitive

nitroveratryloxycarbonyl-caged ROCK inhibitor (caged Y27632; Invitrogen) for 15 min. Caged Y27632 remains inactive until hydrolyzed under UV light (wavelength ≤ 360 nm). To locally activate the compound at a selected dendritic segment (dendrite 1), the microscope pinhole was closed to the minimum, and the selected region was stimulated by a 500-ms exposure to light of short wavelength (band pass filter 360/40 nm). Pictures of the DiI-labeled dendritic tree (absorption of 549 nm and emission of 565 nm) were taken in 1-min intervals. For control purposes, a second dendritic segment (dendrite 2) just outside of the pinhole was observed before and after local uncaging of Y27632 at dendrite 1, and pictures were taken at time points −1 min and +10 min of uncaging at dendrite 1. To verify the specificity of the effects observed after local uncaging of Y27632, we incubated DiI-labeled cells with 0.14% DMSO in HBSS (vector buffer used for caged Y27632) and stimulated selected dendritic segments (dendrite 3) under the same conditions as described for caged Y27632.

Synaptosomal purification

The protocol used to purify synaptosomal fractions from adult rat brain is based on well-established methods used by Cohen et al. (1997) and Carlin et al. (1980). 6 g of adult rat brains were homogenized in 4 vol/g of buffer A (0.32 mM sucrose, 1 mM $MgCl_2$, 0.5 mM $CaCl_2$, 1 mM $NaHCO_3$, chymostatin, leupteptin, antipain, pepstatin, and 1 mM dithiothreitol) at 800 rpm/7 strokes in a Dounce glass homogenizer. After the addition of 10 vol/g of buffer A, the homogenate was centrifuged at 1,400 *g* for 10 min to recover the supernatant S1 and the pellet P1. P1 was resuspended in 4 vol/g of buffer A, homogenized at 800 rpm/3 strokes, and recentrifuged at 700 *g* for 10 min. The resulting supernatant was combined with S1 and centrifuged at 13,800 *g* for 10 min. The obtained supernatant (S2) was separated from the pellet P2 and centrifuged at 100,000 *g* for 1 h. The resulting supernatant (S3) constitutes the cytosolic fraction. P3 was resuspended in 24 ml/10g wet weight of buffer B (0.32 mM sucrose, 1 mM $NaHCO_3$, 1 mM EGTA, 1 mM dithiothreitol, chymostatin, leupeptin, antipain, and pepstatin) and homogenized to obtain the crude synaptosomal fraction. To obtain the pure synaptosomal fraction, the sample was loaded on a discontinuous sucrose gradient (1 and 1.4 M sucrose) and centrifuged for 65 min at 82,500 *g*. The synaptosomal fraction was recovered from the interphase between 1 and 1.4 M sucrose. Protein amount was calculated, and a 4-mg/ml solution was prepared with buffer B. An equal volume of a solution composed of Triton X-100, 0.5 mM Hepes/KOH, and protease inhibitors was added and stirred for 15 min on ice. The sample was centrifuged at 28,000 *g* for 40 min to obtain supernatant LS1. LS1 was centrifuged at 165,000 *g* for 120 min to obtain pellet LP2. LP2 was then homogenized in 2 ml of buffer B and loaded onto a discontinuous sucrose density gradient composed of 1.0, 1.5, and 2.1 M sucrose and was centrifuged at 201,800 *g* for 60 min. A PSD fraction (PSD I) was obtained from the interphase between sample and 1.0 M sucrose.

Protein amounts of the cytosolic, crude syaptosomal fractions were calculated using spectrophotometric analysis. 1.2 ml of PSD I fraction was concentrated to a final volume of 70 μl using chloroform–methanol precipitation. Synaptosomal fractions (500-μl sample volume at 2 mg/ml) were optionally treated with 5- or 55-mM KCl solutions (see next section). Where noted, synaptosomal preparations (500-μl sample volume at 2 mg/ml) were treated with GDP (to 1.0 mM; Pierce Chemical Co.), GTPγS (to 0.1 mM; Pierce Chemical Co.), or ddH_2O (in the case of control experiments). Samples were incubated at 30°C for 30 min under constant agitation, and the reaction was stopped by placing the samples on ice and adding 32 μl of 1 M $MgCl_2$. Activation of NMDA and/or AMPA receptors was performed by incubating synaptosomal preparations with 10 μM NMDA (Sigma-Aldrich) or AMPA (Qbiogene) for 3 min at 37°C under gentle agitation. Optionally, synaptosomal preparations were incubated at 37°C with 1 μM MK-801 (Sigma-Aldrich), 2 μM CNQX (Qbiogene), 100 μM DHPG (Sigma-Aldrich), or 400 μM AIDA (Qbiogene) for 5 min before high potassium treatment (see next section) or incubation with AMPA or NMDA.

KCl treatment

Coverslips were placed into 55 mM KCl (high potassium) buffer (10 mM Hepes, 2.2 mM $CaCl_2$, 0.33 mM Na_2HPO_4, 0.44 mM KH_2PO_4, 4.2 mM $NaHCO_3$, 5.6 mM glucose, 77 mM NaCl, and 55 mM KCl) or 5 mM (low potassium) buffer (10 mM Hepes, pH 7.2, 2.2 mM $CaCl_2$, 0.33 mM Na_2HPO_4, 0.44 mM KH_2PO_4, 4.2 mM $NaHCO_3$, 5.6 mM glucose, 127 mM NaCl, and 5 mM KCl) and incubated for 3 min at 37°C and 5% CO_2 in a humid chamber. Coverslips were then processed for immunofluorescence or replaced into the original growth medium for 22 h (termed 55 mM + wash) before fixation. For synaptosomal preparations, low or high potassium buffer was added to purified samples and incubated at 37°C for 3 min under gentle agitation. These samples were brought to 4°C on ice and used immediately for immunoprecipitation or RhoA activation assay (see below).

RhoA activation assay

Active RhoA was isolated from neuronal lysates and synaptosomal preparations using the EZ-Detect RhoA activation kit (Pierce Chemical Co.). In brief, cell lysates or synaptosomal preparations were incubated with recombinant GST-Rhotekin in the presence of the designated SwellGel Immobilized Glutathione Discs (Pierce Chemical Co.) at 4°C for 1 h (gentle rocking). The column was then centrifuged briefly at 7,200 *g* and washed with washing buffer (25 mM Tris-HCl, pH 7.5, 150 mM NaCl, 5 mM $MgCl_2$, 1% NP-40, 1 mM DTT, and 5% glycerol). The gel-bound active RhoA was eluted by adding 50 μl of sample buffer (125 mM Tris-HCl, pH 6.8, 2% glycerol, 4% SDS, and 0.05% bromophenol blue). The resulting elutes were then used immediately for Western blotting (see below).

Immunoprecipitations

Synaptosomal preparations were precleared with prewashed protein G–Sepharose beads and were incubated with 3 μg anti-RhoA antibody for 1 h at 4°C. Subsequently, protein G–Sepharose beads were added, and samples were incubated overnight at 4°C under gentle rotation. Samples were then washed twice (20 min each) with immunoprecipitation buffer (1% Triton X-100, 100 mM NaCl, 2 mM EDTA, 10 mM Tris-HCl, 1 mM Na_3VO_4, pH 7.5, and protease inhibitors), twice (20 min each) with high salt buffer (same as immunoprecipitation buffer but with 500 mM NaCl and no Triton X-100), and once (20 min) with low salt buffer (same as immunoprecipitation buffer but no NaCl or Triton X-100). Beads were pelleted in between washes by centrifugation at 1,600 *g* for 30 s. After the final wash, beads were pelleted down by high-speed centrifugation, and the supernatant was analyzed by Western blotting (see below).

Western blotting

Approximately 40 μg of cytosolic and pure synaptosomal fraction and 22 μl of concentrated PSD I fraction were loaded on 12% SDS gels and separated by electrophoresis. Separated proteins were transferred to nitrocellulose filters. Filters were blocked by incubation in 3% BSA in PBS with 0.1% Tween-20. Filters were then incubated with the indicated primary antibodies and with the respective secondary HRP-conjugated antibodies (see Antibodies). Signal detection was performed using an ECL detection kit (GE Healthcare) before exposure to photosensitive films. The obtained autoradiogram was scanned at high resolution (3000 Pro Scanner; Epson) and exported for densitometry analysis (see next section) using National Institutes of Health (NIH) Image 1.63 software.

Measurements

Unless noted differently, dendritic spine number was calculated in individual mature hippocampal neurons obtained from three independent experiments ($n = 9$ cells/treatment within one experiment). Labeling F-actin with TRITC-conjugated phalloidin identified dendritic spines. Where noted, double labeling was performed using phalloidin together with antibodies against ST, synaptophysin, or GluR1. A total dendrite length of 40 μM analyzed per cell and dendritic spine number was determined based on the phalloidin. Where applicable, the determination of dendritic spine number also took into consideration only those F-actin protuberances exhibiting apposed presynaptic terminals (as detected with the presynaptic markers). In all cases, the total number of dendritic spines per cell was averaged for each experiment (population). These population means and the respective SDs were then pooled together and plotted as bar graphics in percentages, thus reflecting the mean variation between individual neurons across populations. Analysis within each separate population revealed similar variations, indicating that the pooled population data reflect the variations across individual populations. Multivariate analysis was performed with one-way analysis of variance (ANOVA) followed by Tukey's multiple comparison test (confidence interval = 95%). Signal intensities of proteins (in autoradiogram) detected by Western blot analysis were measured using NIH 1.63 software. Unless noted differently, each experiment was repeated three times independently. Such measurements were individually normalized against the background of each individual autoradiogram and renormalized against the signal obtained with the unrelated protein α-tubulin (CP06; Oncogene Research Products) unless immunoprecipitated or activation assayed where total protein was loaded for each lane analyzed. The resulting individual, normalized signal densities were averaged for each experiment (population). The data were analyzed by paired *t* test (two-tailed distribution and two-sample unequal variance). In case of multivariate tests,

one-way ANOVA followed by Tukey's multiple comparison test (confidence interval = 95%) was performed. The means and SDs of each experiment were pooled together and represented as graphs in percentages.

Online supplemental material

Fig. S1 shows immunofluorescent images of mature hippocampal neurons labeled with TRITC-conjugated phalloidin. The F-actin pattern and its signal intensity are drastically modified in 55 mM KCl-treated neurons in respect to controls. Fig. S2 shows immunoprecipitations from synaptosomes, illustrating the specificity of the interaction between RhoA and GluR1/NMDAR2a. Fig. S3 illustrates that in synaptosomes, AMPA and NMDA mimic the effect of 55 mM KCl on the RhoA-dependent recruitment of ROCK and PIIa. Online supplemental material is available at http://www.jcb.org/cgi/content/full/jcb.200506136/DC1.

We thank Etienne Cassin and Bianca Hellias for technical assistance.

J.S. Da Silva is supported by an FCT/PRAXIS XXI scholarship (Portuguese Ministry of Science and Technology). V. Schubert is a recipient of a Fondazione Cavalieri Ottolenghi predoctoral fellowship. This work is partially supported by the European Union grant LSHM-CT-2003-503330 (APOPIS) to C.G. Dotti.

Submitted: 21 June 2005
Accepted: 28 December 2005

References

Baskys, A., and M. Blaabjerg. 2005. Understanding regulation of nerve cell death by mGluRs as a method for development of successful neuroprotective strategies. *J. Neurol. Sci.* 229-230:201–209.

Blaabjerg, M., L. Fang, J. Zimmer, and A. Baskys. 2003. Neuroprotection against NMDA excitotoxicity by group I metabotropic glutamate receptors is associated with reduction of NMDA stimulated currents. *Exp. Neurol.* 183:573–580.

Bonhoeffer, T., and R. Yuste. 2002. Spine motility. Phenomenology, mechanisms, and function. *Neuron*. 35:1019–1027.

Bradke, F., and C.G. Dotti. 1997. Videomicroscopy of living microinjected hippocampal neurons in culture. *In* Microinjection and Transgenesis: Strategies and Protocols. A. Cid-Arregui and A. Garcia-Carrancà, editors. Springer-Verlag, Berlin, Germany. 81–94.

Carlin, R.K., D.J. Grab, R.S. Cohen, and P. Siekevitz. 1980. Isolation and characterization of postsynaptic densities from various brain regions: enrichment of different types of postsynaptic densities. *J. Cell Biol.* 86:831–845.

Chen, J.C., and E.J. Lang. 2003. Inhibitory control of rat lateral amygdaloid projection cells. *Neuroscience*. 121:155–166.

Cohen, R.S., F. Blomberg, K. Berzins, and P. Siekevitz. 1977. The structure of postsynaptic densities isolated from dog cerebral cortex. I. Overall morphology and protein composition. *J. Cell Biol.* 74:181–203.

Corder, R., D.F. Mason, D. Perrett, P.J. Lowry, V. Clement-Jones, E.A. Linton, G.M. Besser, and L.H. Rees. 1982. Simultaneous release of neurotensin, somatostatin, enkephalins and catecholamines from perfused cat adrenal glands. *Neuropeptides*. 3:9–17.

Da Silva, J.S., M. Medina, C. Zuliani, A. Di Nardo, W. Witke, and C.G. Dotti. 2003. RhoA/ROCK regulation of neuritogenesis via profilin IIa-mediated control of actin stability. *J. Cell Biol.* 162:1267–1279.

Da Silva, J.S., T. Hasegawa, T. Miyagi, C.G. Dotti, and J. Abad-Rodriguez. 2005. Asymmetric membrane ganglioside sialidase activity specifies axonal fate. *Nat. Neurosci.* 8:606–615.

Dillon, C., and Y. Goda. 2005. The actin cytoskeleton: integrating form and function at the synapse. *Annu. Rev. Neurosci.* 28:25–55.

Ehlers, M.D. 2000. Reinsertion or degradation of AMPA receptors determined by activity-dependent endocytic sorting. *Neuron*. 28:511–525.

Fifkova, E., and R.J. Delay. 1982. Cytoplasmic actin in neuronal processes as a possible mediator of synaptic plasticity. *J. Cell Biol.* 95:345–350.

Fischer, M., S. Kaech, D. Knutti, and A. Matus. 1998. Rapid actin-based plasticity in dendritic spines. *Neuron*. 20:847–854.

Goslin, K., and G. Banker. 1991. Rat hippocampal neurons in low-density culture. *In* Culturing Nerve Cells. G. Banker and K. Goslin, editors. MIT Press, Cambridge, MA. 251–281.

Govek, E.E., S.E. Newey, and L. Van Aelst. 2005. The role of the Rho GTPases in neuronal development. *Genes Dev.* 19:1–49.

Hall, A. 1998. Rho GTPases and the actin cytoskeleton. *Science*. 279:509–514.

Halpain, S., A. Hipolito, and L. Saffer. 1998. Regulation of F-actin stability in dendritic spines by glutamate receptors and calcineurin. *J. Neurosci.* 18:9835–9844.

Harris, K.M., and S.B. Kater. 1994. Dendritic spines: cellular specializations imparting both stability and flexibility to synaptic function. *Annu. Rev. Neurosci.* 17:341–371.

Hering, H., and M. Sheng. 2003. Activity-dependent redistribution and essential role of cortactin in dendritic spine morphogenesis. *J. Neurosci.* 23:11759–11769.

Korkotian, E., and M. Segal. 1999. Bidirectional regulation of dendritic spine dimensions by glutamate receptors. *Neuroreport*. 10:2875–2877.

Korkotian, E., and M. Segal. 2001a. Regulation of dendritic spine motility in cultured hippocampal neurons. *J. Neurosci.* 21:6115–6124.

Korkotian, E., and M. Segal. 2001b. Spike-associated fast contraction of dendritic spines in cultured hippocampal neurons. *Neuron*. 30:751–758.

Leung, T., E. Manser, L. Tan, and L. Lim. 1995. A novel serine/threonine kinase binding the Ras-related RhoA GTPase which translocates the kinase to peripheral membranes. *J. Biol. Chem.* 270:29051–29054.

Li, Z., C.D. Aizenman, and H.T. Cline. 2002. Regulation of rho GTPases by crosstalk and neuronal activity in vivo. *Neuron*. 33:741–750.

Luo, L. 2000. Rho GTPases in neuronal morphogenesis. *Nat. Rev. Neurosci.* 1:173–180.

Luo, L. 2002. Actin cytoskeleton regulation in neuronal morphogenesis and structural plasticity. *Annu. Rev. Cell Dev. Biol.* 18:601–635.

Mateos, J.M., R. Benitez, I. Elezgarai, J.J. Azkue, E. Lazaro, A. Osorio, A. Bilbao, F. Donate, R. Sarria, F. Conquet, et al. 2000. Immunolocalization of the mGluR1b splice variant of the metabotropic glutamate receptor 1 at parallel fiber-Purkinje cell synapses in the rat cerebellar cortex. *J. Neurochem.* 74:1301–1309.

Matsui, T., M. Amano, T. Yamamoto, K. Chihara, M. Nakafuku, M. Ito, T. Nakano, K. Okawa, A. Iwamatsu, and K. Kaibuchi. 1996. Rho-associated kinase, a novel serine/threonine kinase, as a putative target for small GTP binding protein Rho. *EMBO J.* 15:2208–2216.

Matus, A. 2000. Actin-based plasticity in dendritic spines. *Science*. 290:754–758.

Matus, A., M. Ackermann, G. Pehling, H.R. Byers, and K. Fujiwara. 1982. High actin concentrations in brain dendritic spines and postsynaptic densities. *Proc. Natl. Acad. Sci. USA*. 79:7590–7594.

Montgomery, J.M., J.C. Selcher, J.E. Hanson, and D.V. Madison. 2005. Dynamin-dependent NMDAR endocytosis during LTD and its dependence on synaptic state. *BMC Neurosci.* 6:48.

Nagerl, U.V., N. Eberhorn, S.B. Cambridge, and T. Bonhoeffer. 2004. Bidirectional activity-dependent morphological plasticity in hippocampal neurons. *Neuron*. 44:759–767.

Nakayama, A.Y., M.B. Harms, and L. Luo. 2000. Small GTPases Rac and Rho in the maintenance of dendritic spines and branches in hippocampal pyramidal neurons. *J. Neurosci.* 20:5329–5338.

Nimchinsky, E.A., B.L. Sabatini, and K. Svoboda. 2002. Structure and function of dendritic spines. *Annu. Rev. Physiol.* 64:313–353.

Sahai, E., and C.J. Marshall. 2002. ROCK and Dia have opposing effects on adherens junctions downstream of Rho. *Nat. Cell Biol.* 4:408–415.

Santos Da Silva, J., V. Schubert, and C.G. Dotti. 2004. RhoA, Rac1, and cdc42 intracellular distribution shift during hippocampal neuron development. *Mol. Cell. Neurosci.* 27:1–7.

Settleman, J. 1999. Rho GTPases in development. *Prog. Mol. Subcell. Biol.* 22:201–229.

Van Aelst, L., and C. D'Souza-Schorey. 1997. Rho GTPases and signaling networks. *Genes Dev.* 11:2295–2322.

Wang, H.G., F.M. Lu, I. Jin, H. Udo, E.R. Kandel, J. de Vente, U. Walter, S.M. Lohmann, R.D. Hawkins, and I. Antonova. 2005. Presynaptic and postsynaptic roles of NO, cGK, and RhoA in long-lasting potentiation and aggregation of synaptic proteins. *Neuron*. 45:389–403.

Waring, M., J. Drappatz, O. Weichel, P. Seimetz, E. Sarri, I. Bockmann, U. Kempter, A. Valeva, and J. Klein. 1999. Modulation of neuronal phospholipase D activity under depolarizing conditions. *FEBS Lett.* 464:21–24.

Yuste, R., and D.W. Tank. 1996. Dendritic integration in mammalian neurons, a century after Cajal. *Neuron*. 16:701–716.